JACS Au
AN OPEN ACCESS JOURNAL OF THE AMERICAN CHEMICAL SOCIETY

pubs.acs.org/jacsau

Article

Calcium Contributes to Polarized Targeting of HIV Assembly Machinery by Regulating Complex Stability

Chandan Kishor, Belinda L. Spillings, Johana Luhur, Corinne A. Lutomski, Chi-Hung Lin, William J. McKinstry, Christopher J. Day, Michael P. Jennings, Martin F. Jarrold, and Johnson Mak*

Cite This: *JACS Au* 2022, 2, 522–530

Read Online

ACCESS | Metrics & More | Article Recommendations | Supporting Information

ABSTRACT: Polarized or precision targeting of protein complexes to their destinations is fundamental to cellular homeostasis, but the mechanism underpinning directional protein delivery is poorly understood. Here, we use the uropod targeting HIV synapse as a model system to show that the viral assembly machinery Gag is copolarized with the intracellular calcium (Ca^{2+}) gradient and binds specifically with Ca^{2+}. Conserved glutamic/aspartic acids flanking endosomal sorting complexes required for transport binding motifs are major Ca^{2+} binding sites. Deletion or mutation of these Ca^{2+} binding residues resulted in altered protein trafficking phenotypes, including (i) changes in the Ca^{2+}–Gag distribution relationship during uropod targeting and/or (ii) defects in homo/hetero-oligomerization with Gag. Mutation of Ca^{2+} binding amino acids is associated with enhanced ubiquitination and a decline in virion release via uropod protein complex delivery. Our data that show Ca^{2+}–protein binding, via the intracellular Ca^{2+} gradient, represents a mechanism that regulates intracellular protein trafficking.

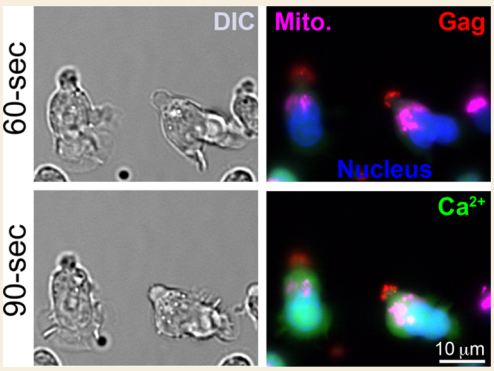

KEYWORDS: *Calcium Sparks, Virological Synapse, Complex Stability, Directional Trafficking, HIV Gag, Protein Oligomerization, Uropod, Polarization*

INTRODUCTION

Directional delivery of protein complexes to their destinations is fundamental to cellular homeostasis, but mechanisms underpinning intracellular protein trafficking are not well-understood. Cell polarity demands a robust yet simple framework to control intracellular cargo movements. This network is vital for cells to expedite responses across biological processes, including (i) firing of neurotransmitters through neurological synapses,[1,2] (ii) dispatching exosomes via exocytosis,[3,4] and (iii) mounting immune responses through immunological synapses.[5,6] In the context of immunity, immune cells may undergo rapid reversing of cell polarity (via reorientation of the microtubule organizing center [MTOC]) to engage with target cells.[5,6] While organelle targeting signals or association with "destination-specific proteins" could explain how proteins reach destinations via hitchhiking "existing" delivery vehicles, these narratives do not, however, account for the logistics of how these delivery systems initiate or redirect cargos toward organelles located in the opposite end of the cells in the first place. As viruses rely on cellular machineries to propagate, the polarized assembly and release of HIV via virological synapses may shed light on the underlying mechanisms of intracellular protein trafficking.

The polarity of cells can be defined based on the relative positioning of the nucleus and MTOC, where the latter is generally found on one side of the nucleus that consists of a higher abundance of endoplasmic reticulum (ER). In fibroblasts, neurons, and epithelial and endothelial cells, the MTOC localizes in front of the nucleus in the direction of migration (leading edge).[7] In contrast, the MTOC in immune cells is generally found in the uropod (retracting end) and reorients itself to sit between the attachment interface (synapse) and the nucleus upon cell–cell engagement.[5,6] Regardless of cell types, MTOC and enrichment of ER are found on the side of the secretory apparatus where vesicles or viruses are released. Due to Ca^{2+} storage in the ER and mitochondrial regulation,[8−13] both an overall and subcellular local Ca^{2+} gradient exists within cells.[8−13] Another common thread among synapse biology and exocytosis events is the involvement of the multivesicular bodies (MVBs) pathway and endosomal sorting complexes required for transport (ESCRT) machineries, which are also exploited by many viruses for assembly and release.[14,15]

Received: December 16, 2021
Published: February 1, 2022

https://doi.org/10.1021/jacsau.1c00563
JACS Au 2022, 2, 522–530

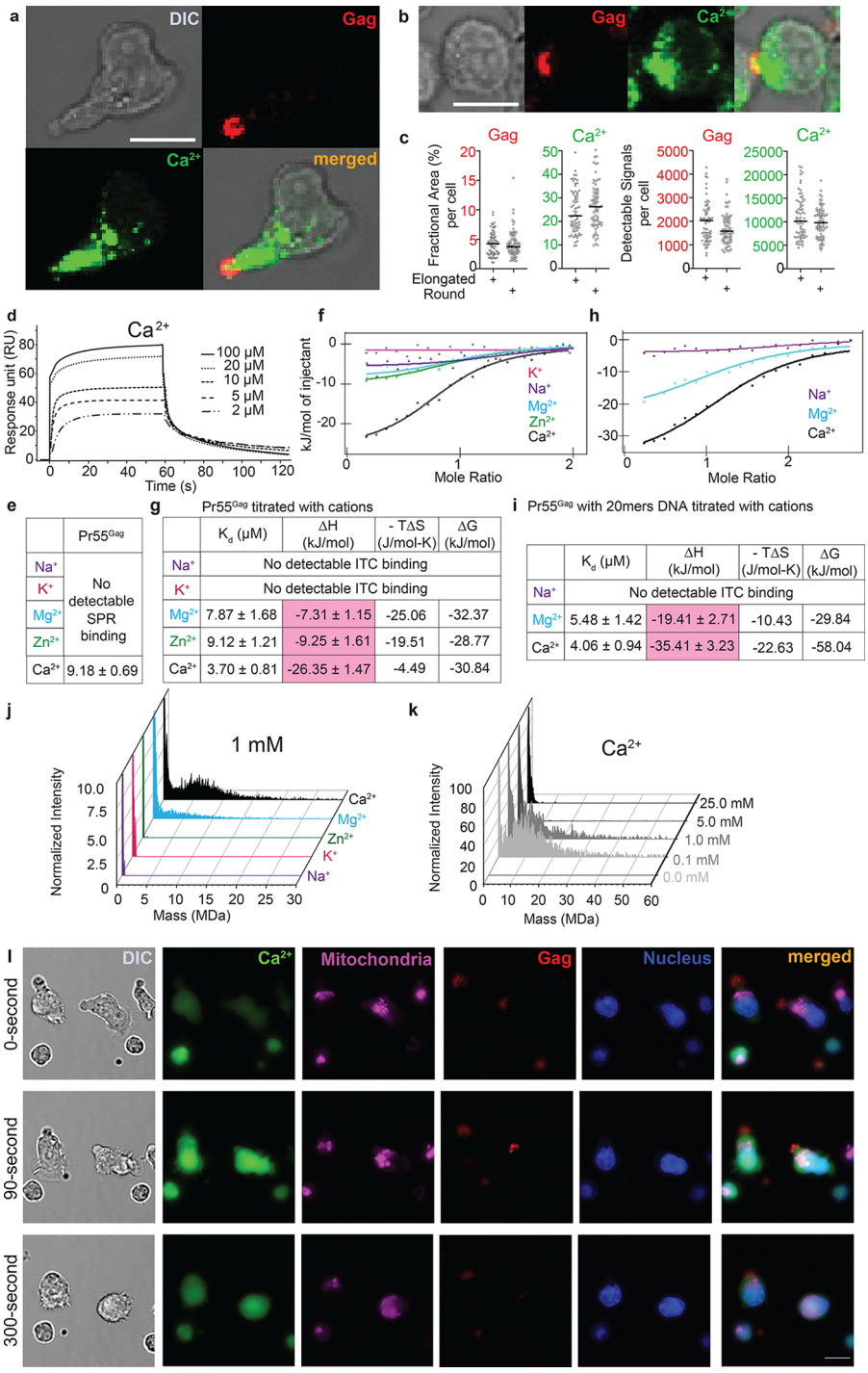

Figure 1. Calcium cation binds specifically to HIV Gag and promotes Gag−Gag assembly. (a,b) Distribution of $Pr55^{Gag}$-imCherry (red) and Ca^{2+} (green) in elongated (a) and round (b) PBLs is shown. DIC, single fluorescent and merged images are included. Scale bar 10 μm. (c) Fractional areas and detectable signals of $Pr55^{Gag}$-imCherry (red) and Ca^{2+} (green) in elongated and round PBLs expressing $Pr55^{Gag}$ are shown. Medians are highlighted (n = 75 cells per arm). (d) Ca^{2+} binds to $Pr55^{Gag}$ in SPR. (e) SPR estimated dissociation constant (K_d) between cations and $Pr55^{Gag}$ are listed (n > 3). (f) ITC binding profiles between $Pr55^{Gag}$ and Ca^{2+} or other cations (Mg^{2+}, Zn^{2+}, Na^{+}, and K^{+}) (n > 3). (g) ITC thermodynamic parameters between $Pr55^{Gag}$ and cation interaction are listed (n > 3). (h) ITC profiles of $Pr55^{Gag}$ binding with cations in the presence of 20 μM of 20mers DNA oligonucleotides (4× 5′-GAGAA-3′) are shown (n > 3). (i) ITC thermodynamic parameters between $Pr55^{Gag}$ and cation in the presence of 20 μM of 20 mers DNA oligonucleotides (4× 5′-GAGAA-3′) are shown (n > 3). (j) CDMS of the assembly reaction of $Pr55^{Gag}$ containing 4:1 molar ratio of $Pr55^{Gag}$/DNA oligonucleotides (4× 5′-GAGAA-3′), plus 2 μM IP5 and 1 mM cationic cofactors, such as Na^{+}, K^{+}, Zn^{2+}, Mg^{2+}, and Ca^{2+}. Ion counts are normalized to 100; the y-axis is truncated to reveal the broad extent of oligomerization (n > 3). (k) CDMS quantification of $Pr55^{Gag}$ oligomerization as a function of Ca^{2+} concentration from the absence of Ca^{2+} (front) to 25 mM Ca^{2+} (rear). Only ions above 500 kDa are shown, and counts are normalized to 100 (n > 3). (l) Distribution of Ca^{2+} (green), mitochondria (magenta), $Pr55^{Gag}$-imCherry (red), and nucleus (blue) in CD4+ T-lymphocytes from three different time points are shown. DIC, single fluorescent and merged images are included. Scale bar 10 μm.

https://doi.org/10.1021/jacsau.1c00563
JACS Au 2022, 2, 522−530

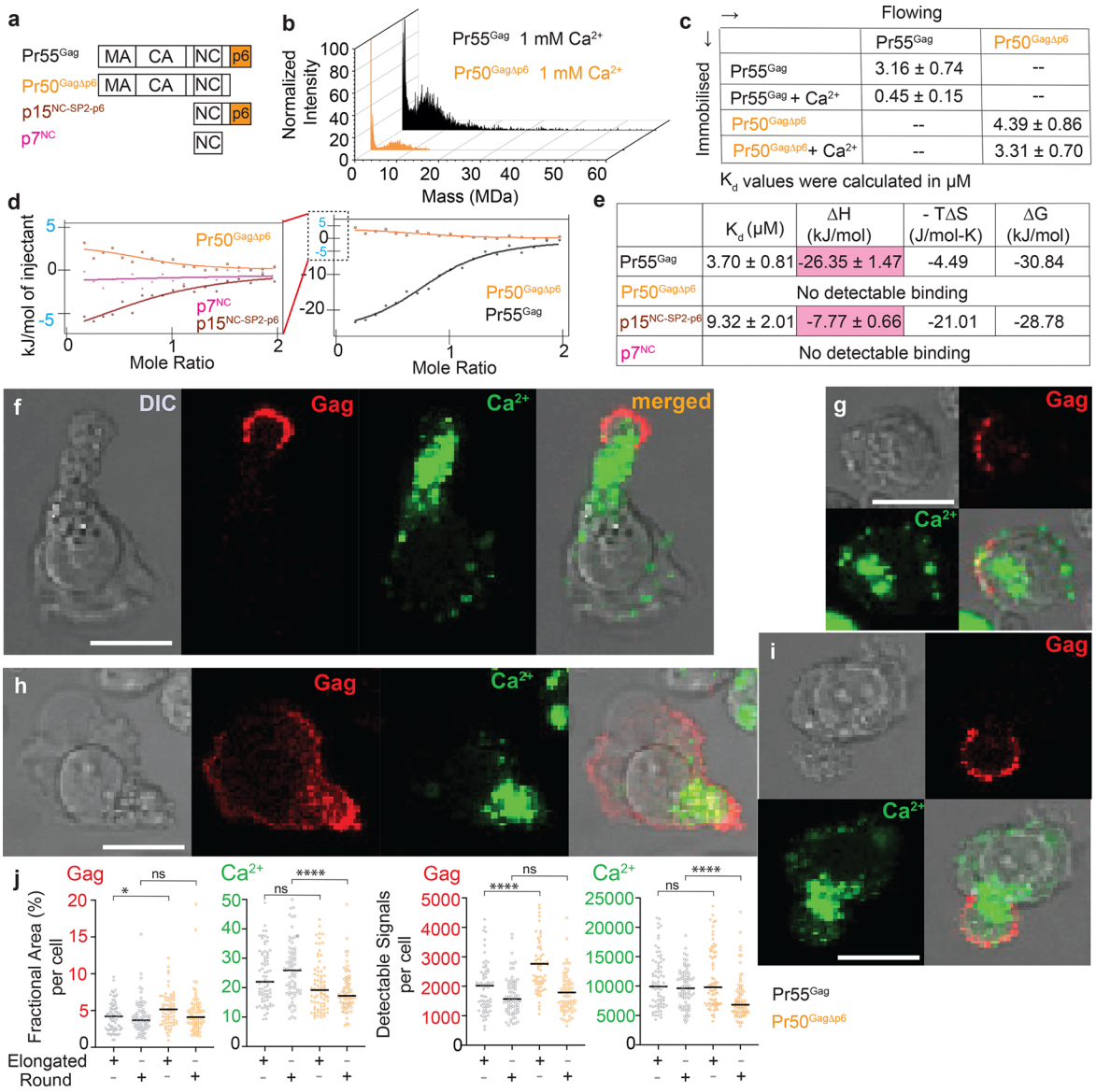

Figure 2. p6^{Gag} is an important determinant of Ca^{2+} binding and enhances Gag−Gag interactions. (a) Schematic shows domains in Pr55^{Gag} and its derivatives (Pr50^{GagΔp6}, p15$^{NC-SP1-p6}$, and p7^{NC}). (b) p6^{Gag} contributes to in vitro Ca^{2+}-induced high-order Gag oligomerization in CDMS (n > 3). (c) Ca^{2+} promotes SPR-detected homodimerization of Pr55^{Gag} but not with Pr50^{GagΔp6} (n > 3). (d) ITC Ca^{2+} binding profiles of Pr55^{Gag} (and its derivatives) show that p6^{Gag} contributes to Ca^{2+} interaction. Zoom-In ITC profiles are presented for p15$^{NC-SP2-p6}$ and p7^{NC} (n > 3). (e) ITC thermodynamic parameters are obtained between Pr55^{Gag} (or its derivatives) and Ca^{2+} (n > 3). (f–i) Distribution of Pr50^{GagΔp6}-imCherry (red) and Ca^{2+} (green) in elongated (f,h,i) and round (g) PBLs are shown. DIC, single fluorescent and merged images are included. Scale bar 10 μm. (j) Fractional areas and detectable signals of Pr50^{GagΔp6}-imCherry (red) and Ca^{2+} (green) in elongated and round PBLs expressing Pr50^{GagΔp6} are shown. Medians are highlighted (n = 75 cells per arm). Statistical distribution analyses against Pr55^{Gag} are with two-sample Kolmogorov−Smirnov test.

RESULTS

Uropod Targeting and Oligomerization of HIV Gag Are Associated with Ca^{2+} Gradient

Uropod targeting or virological synapse formation is conserved among retroviruses,[16−20] and this process is associated with the oligomerization of the retroviral Gag protein.[21] Using HIV virological synapse as a model system, our fluorescent imaging analyses show that the subcellular distributions of HIV Gag (imCherry, modified from ref 22) in peripheral blood lymphocytes (PBLs) are copolarized and overlapped with intracellular Ca^{2+} gradient (fluo-4) both in the elongated and round PBLs (Figures 1a,b and S1). The median area distribution of detectable HIV Gag represented 4.2 and 3.7% of cell areas in the elongated (virological synapses displaying) PBLs and the round (less-extended virological synapse forming) PBLs (Figures 1c and S1), whereas detectable Ca^{2+} occupied 22.0 and 25.9% areas of corresponding PBLs, respectively (Figures 1c and S1). Surface plasmon resonance (SPR) analyses showed recombinant HIV Gag specifically binds to Ca^{2+} with an estimated SPR dissociation constant (K_d) of 9.18 μM (Figures 1d,e and S2 and S3) but has undetectable SPR binding with other cations (Na^+, K^+, Mg^{2+}, and Zn^{2+}; Figures 1e and S3). Isothermal titration calorimetry (ITC) has been used to record the thermodynamics of HIV Gag oligomerization events among low-order Gag oligomers.[23] ITC showed that the inclusion of divalent cations resulted in

https://doi.org/10.1021/jacsau.1c00563
JACS Au 2022, 2, 522−530

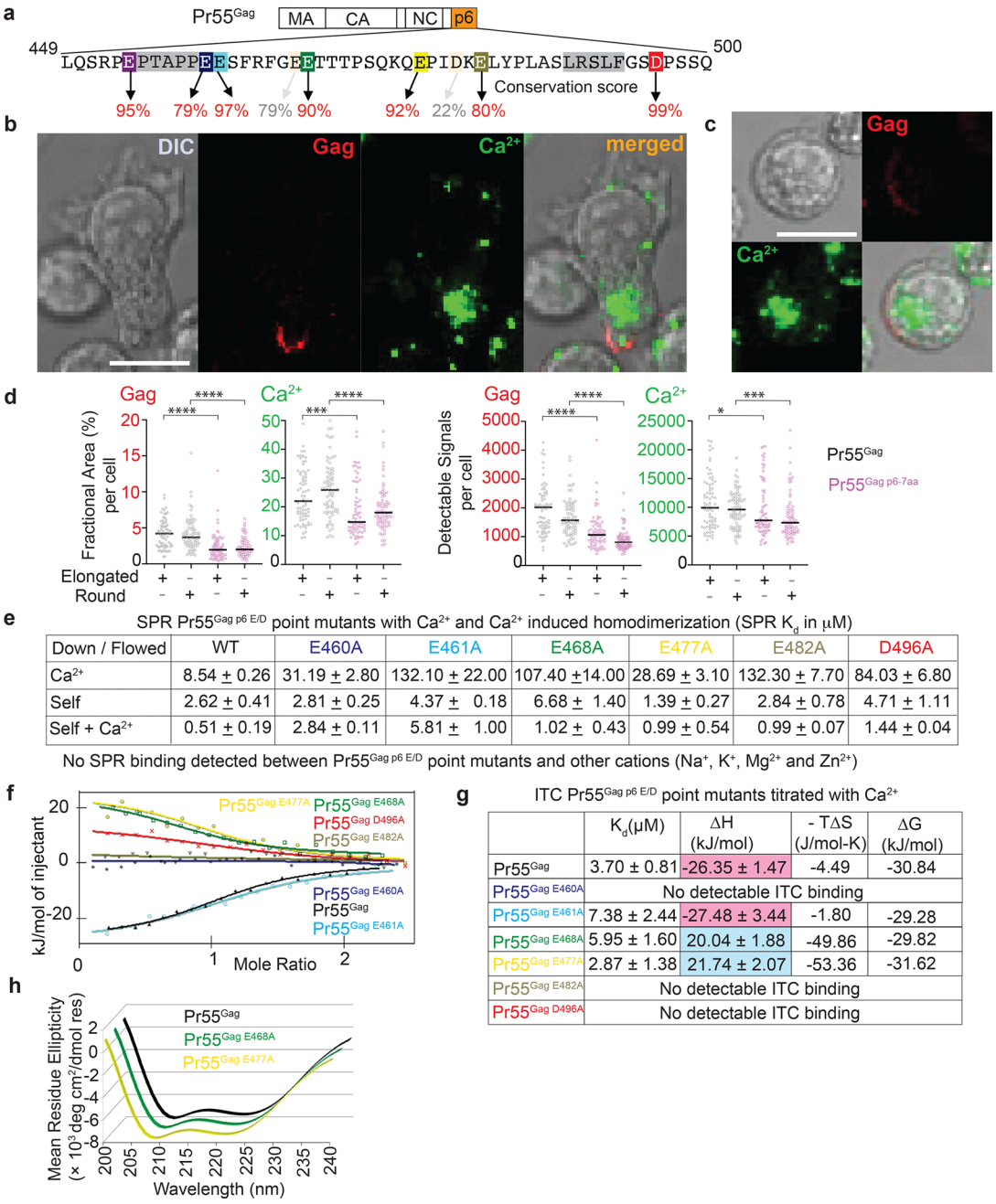

Down / Flowed	WT	E460A	E461A	E468A	E477A	E482A	D496A
Ca^{2+}	8.54 ± 0.26	31.19 ± 2.80	132.10 ± 22.00	107.40 ±14.00	28.69 ± 3.10	132.30 ± 7.70	84.03 ± 6.80
Self	2.62 ± 0.41	2.81 ± 0.25	4.37 ± 0.18	6.68 ± 1.40	1.39 ± 0.27	2.84 ± 0.78	4.71 ± 1.11
Self + Ca^{2+}	0.51 ± 0.19	2.84 ± 0.11	5.81 ± 1.00	1.02 ± 0.43	0.99 ± 0.54	0.99 ± 0.07	1.44 ± 0.04

	K_d(μM)	ΔH (kJ/mol)	- TΔS (J/mol-K)	ΔG (kJ/mol)
$Pr55^{Gag}$	3.70 ± 0.81	-26.35 ± 1.47	-4.49	-30.84
$Pr55^{Gag\ E460A}$	No detectable ITC binding			
$Pr55^{Gag\ E461A}$	7.38 ± 2.44	-27.48 ± 3.44	-1.80	-29.28
$Pr55^{Gag\ E468A}$	5.95 ± 1.60	20.04 ± 1.88	-49.86	-29.82
$Pr55^{Gag\ E477A}$	2.87 ± 1.38	21.74 ± 2.07	-53.36	-31.62
$Pr55^{Gag\ E482A}$	No detectable ITC binding			
$Pr55^{Gag\ D496A}$	No detectable ITC binding			

Figure 3. Conserved $p6^{Gag\ E/D}$ residues influence Ca^{2+}-$Pr55^{Gag}$ interactions. (a) Nine E/D residues in $p6^{Gag}$ are identified. Seven out of nine conserved E/D residues are highlighted in rainbow shadow, and the same color scheme is used for both this figure and Figure 4. Both PTAP and LXXLF motifs are denoted with a gray background. Conservation scores are in red. (b,c) Distribution of $Pr55^{Gag\ p6\text{-}7aa}$-imCherry (red) and Ca^{2+} (green) in elongated (b) and round (c) PBLs is shown. DIC, single fluorescent and merged images are included. Scale bar 10 μm. (d) Fractional areas and detectable signals of $Pr55^{Gag\ p6\text{-}7aa}$-imCherry (red) and Ca^{2+} (green) in elongated and round PBLs expressing $Pr55^{Gag\ p6\text{-}7aa}$ are shown. Medians are highlighted (n = 75 cells per arm). Statistical distribution analyses against $Pr55^{Gag}$ are with a two-sample Kolmogorov−Smirnov test. (e) SPR estimated dissociation constants (K_d) are Ca^{2+} induced homodimerization impacted by Ca^{2+} binding site mutations (n > 3). (f) ITC Ca^{2+} binding profiles of $Pr55^{Gag}$ $p6^{Gag\ E/D}$ point mutants are shown (n > 3). (g) ITC thermodynamic parameters are obtained between $Pr55^{Gag}$ $p6^{Gag\ E/D}$ point mutant and Ca^{2+} (n > 3). (h) CD spectra of recombinant $Pr55^{Gag\ E468A}$ and $Pr55^{Gag\ E477A}$ are shown (n > 3).

energetically favorable reactions (ΔG < 0) during low-order Gag oligomerization over monovalent cations, where Ca^{2+} stimulated the highest change in enthalpy (ΔH) across all cations tested (Figures 1f,g and S4). The Ca^{2+}-induced enhancement (for both ΔG and ΔH) on the low-order Gag oligomerization in ITC was strengthened in the presence of nucleic acids (Figures 1h,i and S4). Charge detection mass spectrometry (CDMS) is a single molecule technique that can quantify high-order oligomerization (~4 MDa [120mers] of hepatitis B viral proteins) in vitro.[24,25] CDMS analyses showed that in vitro high-order oligomerization of HIV Gag (with a median of 7−12 MDa [125−220mers]) is promoted by Ca^{2+} (Figures 1j and S5) with optimal Ca^{2+} concentrations ($[Ca^{2+}]$) at 0.1−1.0 mM (Figures 1k and S5) that mirrors the high end of intracellular Ca^{2+} gradient. The lower "overall" 100 nM cytoplasmic $[Ca^{2+}]$ is in sharp contrast with the $[Ca^{2+}]$ needed

https://doi.org/10.1021/jacsau.1c00563
JACS Au 2022, 2, 522−530

to induce HIV Gag oligomerization. Whether it is known as "sparks" in muscle cells,[26−28] "puffs" in oocytes,[29] or "syntillas" in neurons,[30] high [Ca^{2+}] can be transiently released locally via intracellular organelles, such as mitochondria, ER, and acidic vacuoles.[31] The local [Ca^{2+}] in these storage compartments can reach 100−800 μM,[31] which is sufficient to support the oligomerization of HIV Gag during its trafficking to virological synapses. Our time-lapse live imaging showed that stochastic Ca^{2+} sparks occur among T-lymphocytes, and the two selected T-lymphocytes displayed spikes of Ca^{2+} signals (via fluo-4 complex) at ∼90 s with a slow decay of the Ca^{2+} signal (Figure 1l and Videos S1−S6). A combination of (i) super-resolution microscopy, (ii) 3D volume imaging, (iii) time-lapse video, and (iv) alternative Ca^{2+} dye to distinguish the flux (blink) of Ca^{2+} will be needed to define the details of the temporal and spatial relationship between local Ca^{2+} release and intracellular trafficking of Gag.

C-Terminus p6 Domain of HIV Gag Is a Determinant of Ca^{2+}-Associated In Vitro Gag−Gag Interaction and Intracellular Trafficking

The capsid (CA) domain within HIV Gag (Figure 2a) drives viral assembly by facilitating homo-oligomerization of Gag molecules,[32,33] and in vitro assembly of virus-like-particles can occur in the absence of p6.[34] Deletion of p6 from recombinant HIV Gag drastically reduced the quantity and the size of CDMS-detectable Ca^{2+}-induced high-order HIV Gag oligomers (Figure 2b). SPR revealed that Gag−Gag homo-dimerization was strengthened up to 7-fold in the presence of Ca^{2+} with SPR K_d (Figures 2c and S6), but this Ca^{2+}-induced homodimerization effect disappeared when the p6 domain was removed (Figures 2c and S6). The ITC-detected Ca^{2+} binding during low-order Gag oligomerization also vanished in the absence of p6 (Figures 2d,e and S7). As the energy exchange detected in ITC low-order Gag oligomerization is contributed in part by CA−CA-based interactions,[23] ITC analyses with $p15^{NC\text{-}SP2\text{-}p6}$ and $p7^{NC}$ (lacking the $p39^{MA\text{-}CA\text{-}Sp1}$ domains, Figure 2a) have mapped that the $p6^{Gag}$ domain directly contributes to Ca^{2+} binding (Figures 2d,e and S7).

If the Ca^{2+}−$p6^{Gag}$ interaction is important for intracellular trafficking of HIV Gag, removal of $p6^{Gag}$ should alter the relationship between Ca^{2+} and HIV Gag during virological synapse formation. In virological synapse displaying elongated PBLs, cell imaging analyses showed that the p6-deleted HIV Gag had a more dispersed distribution and occupied a greater fractional area when compared with that of wild-type HIV Gag (Figures 2f,h−j and S8). In contrast, the intracellular Ca^{2+} distributions were generally more condensed within a smaller fractional area of $Pr50^{Gag\Delta p6}$ expressing cells than $Pr55^{Gag}$ expressing cells, a phenotype that is more noticeable in the less extended virological synapse forming round PBLs (Figures 2g,j and S8). In elongated PBLs, an increase in Gag signal was detected in $Pr50^{Gag\Delta p6}$- over $Pr55^{Gag}$-expressing cells (Figures 2f,h−j and S8), while no difference in overall Gag signal was found between $Pr50^{Gag\Delta p6}$ and $Pr55^{Gag}$ round PBLs (Figures 2g,j and S8). The signal strength ratio of Gag to Ca^{2+} was consistently higher in $Pr50^{Gag\Delta p6}$- than in $Pr55^{Gag}$-expressing cells across all PBLs (Figures 2f−j and S8). The altered Ca^{2+}−Gag distribution relationship between $Pr50^{Gag\Delta p6}$- and $Pr55^{Gag}$-expressing cells could be related to a nonsynchronous lateral movement of the Ca^{2+} gradient and viral proteins during the re-establishment of virological synapses from the virus-laden uropod.[16] Our data support the notion that a relationship exists between the intracellular Ca^{2+} and the p6 domain of HIV Gag that contributes to the intracellular trafficking of HIV Gag for directional release.

Conserved Glutamic/Aspartic Acids Flanking HIV ESCRT Binding Motifs Are Ca^{2+} Binding Sites Involved in HIV Gag Trafficking

Ca^{2+} often acts as a coordination point that interacts with multiple oxygen atoms from the carbonyl group of amino acids with negatively charged side chains (such as glutamic (E)/aspartic (D) acids) to stabilize intra- or intermolecule interactions.[35−37] Point mutations were introduced into 7 out of 9 of the most conserved E/D residues within the $p6^{Gag}$ to generate the $Pr55^{Gag\ p6\text{-}7aa}$ mutant (Figure 3a [red conservation scores]). Imaging analyses showed that $Pr55^{Gag\ p6\text{-}7aa}$ occupied half of the fractional area and exhibited half of the signal intensity as seen with wild-type $Pr55^{Gag}$ (Figures 3b−d and S9). Consistent with a role of direct Ca^{2+} binding in HIV Gag trafficking, both the fractional area occupied and the signal intensity displayed of Ca^{2+} were significantly lower in $Pr55^{Gag\ p6\text{-}7aa}$-expressing cells in comparison with those of wild-type $Pr55^{Gag}$-expressing cells (Figures 3b−d and S9). A single alanine point mutation was independently introduced into 6 of the putative Ca^{2+} binding sites within the recombinant HIV Gag. Biophysical analyses showed that all 6 recombinant $Pr55^{Gag}$ point mutants displayed between 3- and 15-fold reduction in Ca^{2+} SPR binding (Figures 3e and S10), and the enhancement of Ca^{2+}-induced Gag−Gag homodimerization in SPR was either reduced or eliminated in 5 out of 6 recombinant $Pr55^{Gag}$ point mutants (Figures 3e and S10). Fluorescent imaging and SPR data supported a role of $p6^{Gag\ E/D}$ residues in Ca^{2+} binding to facilitate intracellular trafficking. The individual contributions of these mutations on Ca^{2+} binding during low-order Gag oligomerization were independently examined by ITC. Apart from $Pr55^{Gag\ E461A}$ that registered indistinguishable thermodynamic properties compared to wild-type $Pr55^{Gag}$, 3 out of 6 mutants ($Pr55^{Gag\ E460A}$, $Pr55^{Gag\ E482A}$, and $Pr55^{Gag\ D496A}$) showed no ITC detectable Ca^{2+} binding in low-order Gag−Gag homo-oligomerization in vitro (Figures 3f,g and S11). While mutant $Pr55^{Gag\ E468A}$ and $Pr55^{Gag\ E477A}$ retained their in vitro ITC-detectable Ca^{2+} binding, the thermodynamic properties of these Ca^{2+}−Gag homo-oligomer interactions were reversed from a wild-type exothermic reaction to endothermic reactions in these mutants (Figures 3f,g and S11). Circular dichroism showed that $Pr55^{Gag\ E468A}$ and $Pr55^{Gag\ E477A}$ maintained the same overall α-helix and β-sheet contents of $Pr55^{Gag}$ (Figure 3h). These data support a role for E/D amino acid residues flanking the ESCRT motifs in the HIV $p6^{Gag}$ as Ca^{2+} binding sites during HIV Gag trafficking. Production of recombinant $Pr55^{Gag}$ with more than one Ca^{2+} binding site mutations was not successful thus far, making it difficult to further dissect the biophysical properties $Pr55^{Gag}$ containing combined Ca^{2+} binding site mutations using cell-free assays.

Ca^{2+} Binding Stabilizes HIV Gag Assembly Complexes for Directional Trafficking and Release

Reduction of fluorescent signals of $Pr55^{Gag\ p6\text{-}7aa}$ suggests that the stability of the HIV protein complex (such as the homo-oligomerization of Gag) might be compromised without wild-type Ca^{2+} binding (Figures 3b−d and S9). As ubiquitination is both important in HIV biology[38,39] and a post-translational protein degradation system,[40] we examined the impact of changes in Ca^{2+} binding on the ubiquitination of HIV Gag

https://doi.org/10.1021/jacsau.1c00563
JACS Au 2022, 2, 522−530

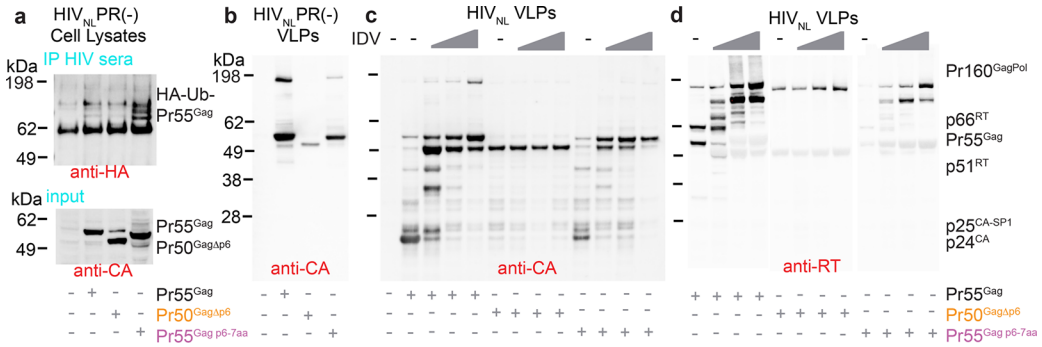

e Infectivity of full-length HIV$_{NL}$ with Pr55$^{Gag\ p6\ E/D}$ mutation(s)

	E454G	E460G	E461G	E468G	E477G	E482G	D496G	E468G + E477G	E482G + D496G
MT2, n=2	NDC	NDC	NDC	NDC	NDC	NDC	NDC	≥ 27-fold reduction	NDC
PBLs, n=3	NDC	NDC	NDC	NDC	NDC	NDC	NDC	≥ 25-fold reduction	NDC

NDC: No Detectable differences from parental wild type control

f-i Virion protein profiles of full-length HIV with Pr55$^{Gag\ p6\ E/D}$ mutants

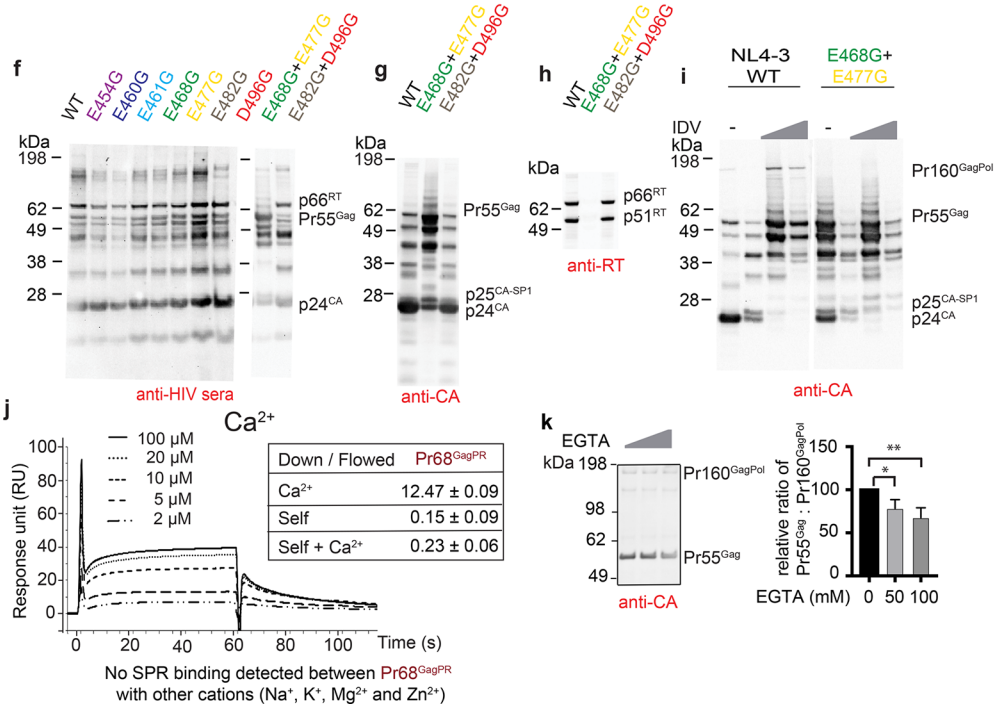

Figure 4. p6^{Gag} Ca^{2+} binding sites contribute to homo/hetero-oligomerization of proteins. (a) Ubiquitination of Pr55^{Gag} is associated with Ca^{2+} binding site mutations ($n > 3$). (b) Deletion of p6^{Gag} and mutations of p6^{Gag} Ca^{2+} binding sites reduces particle release ($n > 3$). (c,d) Deletion of p6^{Gag} and mutations of p6^{Gag} Ca^{2+} binding sites are associated with defects in Pr55^{Gag} processing and Pr160^{GagPol} packaging. Increasing concentrations of indinavir (at 0, 0.5, 5, 50 μM) are used to slow down Pr160^{GagPol}-mediated proteolytic processing ($n > 3$). (e) Relative infectivity of p6^{Gag} Ca^{2+} binding site mutants against wild-type control are shown for T-cell line and PBLs. (f) Virion protein profiles among wild-type (NL4-3^{WT}) and mutant HIV (NL4-3^{E454G}, NL4-3^{E460G}, NL4-3^{E461G}, NL4-3^{E468G}, NL4-3^{E477G}, NL4-3^{E482G}, NL4-3^{E496G}, NL4-3$^{E468G+E477G}$, and NL4-3$^{E482G+E496G}$). HIV patient sera is the source of antibodies ($n > 3$). (g,h) Virion protein profiles of dual mutants (NL4-3$^{E468G+E477G}$ and NL4-3$^{E482G+E496G}$) in comparison with NL4-3^{WT}. Virion proteins are probed with anti-p24^{CA} (g) and anti-p66/51^{RT} (h) antibodies. (i) Virion-associated Pr160^{GagPol} are compared between NL4-3^{WT} and NL4-3$^{E468G+E477G}$ particles that have been produced with increasing concentrations of the viral protease inhibitor indinavir (at 0, 0.5, 5, 50 μM). Virion proteins are probed with anti-p24^{CA} ($n > 3$). (j) SPR analyses of Ca^{2+}–Pr68^{GagPR} binding and effects of Ca^{2+} on Pr68^{GagPR} homodimerization ($n > 3$). (k) Coimmunoprecipitation on the stability of Pr55^{Gag}/Pr160^{GagPol} complexes in the presence of EGTA and quantifications of relative Pr55^{Gag}/Pr160^{GagPol} ratio ($n > 3$).

protein complexes. Immunoprecipitation of Pr55^{Gag} showed that an increased level of ubiquitination was detected in Ca^{2+}-binding-repressed Pr55$^{Gag\ p6\text{-}7aa}$ (Figure 4a). As p6^{Gag} is a major segment for HIV Gag ubiquitination,[38,41] deletion of p6^{Gag} has reduced detectable ubiquitinated Pr50^{GagΔp6} (Figure 4a). Virological assays were used as a surrogate to quantify the functional impacts of interfering with Ca^{2+} interactions on directional trafficking of proteins in cells. Particle release from a protease inactive (PR[-] via PR^{D25G} mutation) and an envelope negative immature virus-like particle (VLP) system (HIV$_{NL}$ GagPol PR[-], modified from ref 42) was used for direct comparison for uropod targeting of HIV Gag oligomeric complexes. Equivalent volumes of viral particle supernatants were pelleted for Western blot analyses. A lower number of

https://doi.org/10.1021/jacsau.1c00563
JACS Au 2022, 2, 522−530

pelleted particles was detected upon in-frame deletion of $p6^{Gag}$ (HIV_{NL} GagPol $Gag^{\Delta p6}$ PR[-]) (Figure 4b), which was in part due to ESCRT-related membrane arrest of particle release. Lower levels of immature $Pr55^{Gag\ p6\text{-}7aa}$ VLPs (HIV_{NL} GagPol $Gag^{p6\text{-}7aa\ (E/D\text{-}G)}$ PR[-]) supported the notion that Ca^{2+} binding site mutations were defective in uropod particle targeting (Figure 4b), implying that the Ca^{2+}-mediated Gag−Gag homo-oligomerization is a determinant of directional trafficking of HIV protein complexes in cells. Previous analyses with a different combination of glutamic acids mutations in $p6^{Gag}$ reported a similar ubiquitination-mediated degradation of HIV Gag.[43]

The principle of direct Ca^{2+} binding to regulate homo-oligomerization of proteins during trafficking should be applicable to hetero-oligomerization of protein complexes, that is, Ca^{2+}-dependent interaction between Gag and non-Gag proteins. The copackaging of virion-associated proteins provides an opportunity to interrogate the role of Ca^{2+} binding on hetero-oligomerization of proteins during the trafficking and the release of HIV particles. HIV GagPol ($Pr160^{GagPol}$) is a well-characterized cotrafficking and copackaging virion-associated protein.[32,33,44] $Pr160^{GagPol}$ represents 10% of the total virion protein[45] and is understood to be packaged into Gag particles via interactions across the mutually shared CA domain between Gag and GagPol.[32,33] Unlike the $p6^{Gag}$ in $Pr55^{Gag}$, the amino acids of $p6^{Pol}$ in $Pr160^{GagPol}$ have a different protein sequence due to overlapping reading frames. $Pr50^{GagΔp6}$ and $Pr55^{Gag\ p6\text{-}7aa}$ were introduced into protease active HIV-1_{NL} GagPol constructs.[42] The proteolytic processing of $Pr50^{GagΔp6}$ was compromised due to deletion of both $p6^{Pol}$ and part of PR (Figure 4c, lane 2 vs lane 6). Site-specific mutations of E/D to G mutations in $Pr55^{Gag\ p6\text{-}7aa}$ via codon modifications have not altered the amino acid sequences of $p6^{Pol}$ of HIV_{NL} GagPol $Gag^{p6\text{-}7aa\ (E/D\text{-}G)}$. The higher ratio of p25/24 CA doublets in $Pr55^{Gag\ p6\text{-}7aa}$ particles compared to that in wild-type $Pr55^{Gag}$ particles suggested that a defect of virion protein maturation may exist in the mutant HIV_{NL} GagPol $Gag^{p6\text{-}7aa\ (E/D\text{-}G)}$ (Figure 4c, lane 2 vs lane 10). Western blot analyses of pelleted particles produced under increased concentrations of the protease inhibitors indinavir (IDV) supported the notion that the defects in $Pr55^{Gag\ p6\text{-}7aa}$ particles could be related to reduction in virion packaging of $Pr160^{GagPol}$ (Figure 4c,d [anti-CA] and [anti-RT], respectively).

Fine mutational analyses were performed to separate out Ca^{2+} binding site mutations that induced complex instability of Gag homo-oligomers (reduction in virion particle release) from the potential defect of Gag−GagPol hetero-oligomerization (suppression in virion packaging of $Pr160^{GagPol}$). Seven single-point mutations and two double-point mutations were introduced into infectious $HIV_{NL4\text{-}3}$. One mutant ($HIV^{Gag\ E468G+E477G}$) was identified to be noninfectious in both T-cell line (MT2) and PBLs (Figure 4e). Although all mutants have wild-type levels of particle release (i.e., no detectable functional impact on Gag−Gag homo-oligomerization), $HIV^{Gag\ E468G+E477G}$ exhibited virion protein processing profile defects (Figure 4f) reminiscent of HIV_{NL} GagPol $Gag^{p6\text{-}7aa\ (E/D\text{-}G)}$ (Figure 4c,d, [anti-CA] and [anti-RT], respectively). The lack of functional impact from the seven single-point mutants (Figure 4e,f) and one double-point mutant ($HIV^{Gag\ E482G+D496G}$, Figure 4e,f) suggests the redundant nature of these Ca^{2+} binding sites in viral replication, which is consistent with the known role of multiple contact points that Ca^{2+}-based interactions often need to stabilize protein complexes. Western blot virion analyses of the double-point mutant ($HIV^{Gag\ E468G+E477G}$) particles with specific anti-HIV antibodies confirmed a defect in virion $Pr55^{Gag}$ processing (Figure 4g) and a reduction of virion-associated polymerase−reverse transcriptase (Figure 4h). Unlike $Pr55^{Gag\ p6\text{-}7aa}$ particles (Figure 4b), the defects in $HIV^{Gag\ E468G+E477G}$ were not associated with impeded viral particle release (i.e., homo-oligomerization of Gag). Inclusion of virion protease inhibitor IDV during particle production confirmed that $HIV^{Gag\ E468G+E477G}$ was defective in virion $Pr160^{GagPol}$ packaging (Figure 4i), showing that the suppression of Ca^{2+} binding via $Pr55^{Gag}$ can lead to reduced hetero-oligomerization of $Pr55^{Gag}$−$Pr160^{GagPol}$ complexes during directional trafficking to the uropod for virion release. To illustrate that $Pr160^{GagPol}$ can directly interact with Ca^{2+}, a recombinant $Pr160^{GagPol}$ surrogate, $Pr68^{GagPR}$, was made by engineering mutations in both the $Pr160^{GagPol}$ frameshift site and the protease active site to express $Pr68^{GagPR}$, consisting of the natural $Pr160^{GagPol}$ domains from $p17^{MA}$ to $p12^{PR[-]}$. SPR analyses showed that $Pr68^{GagPR}$ bound to Ca^{2+} specifically without detectable binding against other cations tested (Figures 4j and S12). To directly examine whether Ca^{2+} can stabilize $Pr55^{Gag}$−$Pr160^{GagPol}$ complexes (hetero-oligomerization), coimmunoprecipitation analyses of immature virus-like particles were done with the divalent cation chelating agent EGTA (or EDTA) via an anti-FLAG antibody and C-terminus FLAG-tagged $Pr160^{GagPol}$ containing virion particles. A dose-dependent reduction of detectable $Pr55^{Gag}$ was seen in the presence of increasing concentrations of EGTA, Ca^{2+} preferred chelating agent, or EDTA (Figures 4k and S12), supporting the notion that direct Ca^{2+} interaction is a mechanism that regulates hetero-oligomerization of HIV $Pr55^{Gag}$−$Pr160^{GagPol}$ complexes during trafficking for directional virion release.

DISCUSSION

The intracellular landscape afforded by the local and overall Ca^{2+} gradient may provide part of the traffic control accounting for the logistics of directional protein−complex movement within the intracellular terrain. Our data provide supportive evidence that both the formation and the trafficking of HIV protein complexes are facilitated in part by direct Ca^{2+} binding. Manipulation of Ca^{2+} binding has resulted in changes in the precision of movement during directional targeting of viral proteins, including association with the post-translational ubiquitination protein degradation regulatory system.[40] In contrast to the well-established Gag oligomerization domain in CA that is known to be critical in Gag−Gag homo-oligomerization and Gag−GagPol hetero-oligomerization,[32,33] our identified Ca^{2+} binding sites in $p6^{Gag}$ that facilitate HIV complex formation were previously not known to be involved in mediating protein oligomerization (homo/hetero). In the context of retroviruses, these data fundamentally change our understanding of retroviral assembly and virion packaging of retroviral GagPol. Moreover, our demonstrated roles of Ca^{2+} to stabilize both homo-oligomerization and hetero-oligomerization in HIV protein complexes could be a generic mechanism that extends beyond HIV biology, given that similar putative Ca^{2+} binding sites are highly conserved amino acids flanking ESCRT binding motifs within retroviral Gag plus the fact that ESCRT machineries are utilized by many viruses to facilitate viral assembly and release.[14,15] Although a role of direct Ca^{2+} binding has not been previously shown to mediate protein trafficking, the contributions of Ca^{2+} to the processes involving

https://doi.org/10.1021/jacsau.1c00563
JACS Au 2022, 2, 522−530

ESCRT-mediated vesicle transport[46] and synaptic vesicle exocytosis[47] are well-documented. Since a single Ca^{2+} cation has the capacity to interact with multiple carbonyl oxygens in amino acids with negatively charged side chains thereby stabilizing (or destabilizing) intra- and interprotein interactions,[35] it is plausible that a series of Ca^{2+}-mediated interactions can exert rigorous control to regulate intracellular protein movement. In the context of HIV and ESCRT-dependent viruses, such a mechanism may allow viral complexes to detour away from the MVB−lysosome degradation pathway for viral particle assembly and release. In a manner analogous to the execution principles in decision-making procedures that are well-known in computational binary processing, whereby a series of on/off events can work together to execute complex tasks with a high degree of accuracy and efficiency, this direct Ca^{2+} binding trafficking strategy has the likelihood to be broadly applicable to the regulation of protein trafficking across all cells that have an intracellular Ca^{2+} gradient.

■ ASSOCIATED CONTENT

Supporting Information

The Supporting Information is available free of charge at https://pubs.acs.org/doi/10.1021/jacsau.1c00563.

Additional materials and methods details and Figures S1−S12 (PDF)

Time-lapse videos of CD4+ T-lymphocytes expressing HIV Gag with 10 s intervals for 10 min that are separated into single fluorescent 326 channels: DIC (AVI), calcium (AVI), mitochondria (AVI), Gag-imCherry (AVI), nucleus 327 (AVI), and merged (AVI) (scale bar is 10 μm)

■ AUTHOR INFORMATION

Corresponding Author

Johnson Mak − *Institute for Glycomics, Griffith University, Gold Coast, QLD 4222, Australia;* orcid.org/0000-0002-5229-5707; Email: j.mak@griffith.edu.au

Authors

Chandan Kishor − *Institute for Glycomics, Griffith University, Gold Coast, QLD 4222, Australia*

Belinda L. Spillings − *Institute for Glycomics, Griffith University, Gold Coast, QLD 4222, Australia*

Johana Luhur − *Institute for Glycomics, Griffith University, Gold Coast, QLD 4222, Australia;* orcid.org/0000-0001-5156-1113

Corinne A. Lutomski − *Department of Chemistry, Indiana University, Bloomington, Indiana 47405, United States;* orcid.org/0000-0001-7509-103X

Chi-Hung Lin − *Institute for Glycomics, Griffith University, Gold Coast, QLD 4222, Australia*

William J. McKinstry − *CSIRO Manufacturing, Parkville, VIC 3004, Australia*

Christopher J. Day − *Institute for Glycomics, Griffith University, Gold Coast, QLD 4222, Australia*

Michael P. Jennings − *Institute for Glycomics, Griffith University, Gold Coast, QLD 4222, Australia;* orcid.org/0000-0002-1027-4684

Martin F. Jarrold − *Department of Chemistry, Indiana University, Bloomington, Indiana 47405, United States;* orcid.org/0000-0001-7084-176X

Complete contact information is available at: https://pubs.acs.org/10.1021/jacsau.1c00563

Author Contributions

Co-first authors: C.K., B.L.S., J.L. (these authors contribute equally). Conceptualization: J.M. Methodology: C.K., B.L.S., J.L., C.A.L., C.-H.L., W.J.Mc.K., C.J.D., J.M. Investigation: C.K., B.L.S., J.L., C.A.L., C.-H.L., C.J.D., J.M. Visualization: C.K., B.L.S., J.L., C.A.L., C.-H.L., C.J.D., J.M. Funding acquisition: B.L.S., M.P.J., M.F.J., J.M. Project administration: J.M. Supervision: M.F.J., J.M.Writing of the original draft: C.K., B.L.S., J.M. Writing, review and editing: C.K., B.L.S., J.L., C.A.L., C.-H.L., W.J.Mc.K., C.J.D., M.P.J., M.F.J., J.M.

Funding

Advance Queensland IRF AQIRS050-2020 (B.L.S.); US National Science Foundation CHE-1531823 (M.F.J.); Australian National Health and Medical Research Council (NHMRC) principal Research Fellowship 1138466 (M.P.J.), Project Grant 1121697 (J.M.).

Notes

The authors declare no competing financial interest.

■ ACKNOWLEDGMENTS

We thank Theodora Hatziioannou and Paul Bieniasz at The Rockefeller University for the HIV_{NL} GagPol VLP expression vector. We thank Barbara Müller and Hans-Georg Kräusslich at Universität Heidelberg for the HA-Ub expression vector. We thank Anthony K. Chen at Peking University for the fluorescent Gag (pNL43ΔPolΔEnv-Gag-mEOS2) expression vector.

■ REFERENCES

(1) Janas, A. M.; Sapon, K.; Janas, T.; Stowell, M. H.; Janas, T. Exosomes and other extracellular vesicles in neural cells and neurodegenerative diseases. *Biochim. Biophys. Acta* **2016**, *1858* (6), 1139−51.

(2) Von Bartheld, C. S.; Altick, A. L. Multivesicular bodies in neurons: distribution, protein content, and trafficking functions. *Prog. Neurobiol* **2011**, *93* (3), 313−40.

(3) Meldolesi, J. Exosomes and Ectosomes in Intercellular Communication. *Curr. Biol.* **2018**, *28* (8), R435−R444.

(4) Cocucci, E.; Meldolesi, J. Ectosomes and exosomes: shedding the confusion between extracellular vesicles. *Trends Cell Biol.* **2015**, *25* (6), 364−72.

(5) Stinchcombe, J. C.; Griffiths, G. M. Secretory mechanisms in cell-mediated cytotoxicity. *Annu. Rev. Cell Dev Biol.* **2007**, *23*, 495−517.

(6) Huppa, J. B.; Davis, M. M. T-cell-antigen recognition and the immunological synapse. *Nat. Rev. Immunol* **2003**, *3* (12), 973−83.

(7) Etienne-Manneville, S. Microtubules in cell migration. *Annu. Rev. Cell Dev Biol.* **2013**, *29*, 471−99.

(8) Morlino, G.; Barreiro, O.; Baixauli, F.; Robles-Valero, J.; Gonzalez-Granado, J. M.; Villa-Bellosta, R.; Cuenca, J.; Sanchez-Sorzano, C. O.; Veiga, E.; Martin-Cofreces, N. B.; Sanchez-Madrid, F. Miro-1 links mitochondria and microtubule Dynein motors to control lymphocyte migration and polarity. *Mol. Cell. Biol.* **2014**, *34* (8), 1412−26.

(9) Giorgi, C.; Marchi, S.; Pinton, P. The machineries, regulation and cellular functions of mitochondrial calcium. *Nat. Rev. Mol. Cell Biol.* **2018**, *19* (11), 713−730.

(10) Duchen, M. R. Mitochondria and calcium: from cell signalling to cell death. *J. Physiol* **2000**, *529* (1), 57−68.

(11) Verkhratsky, A. Physiology and pathophysiology of the calcium store in the endoplasmic reticulum of neurons. *Physiol Rev.* **2005**, *85* (1), 201−79.
(12) Rizzuto, R.; De Stefani, D.; Raffaello, A.; Mammucari, C. Mitochondria as sensors and regulators of calcium signalling. *Nat. Rev. Mol. Cell Biol.* **2012**, *13* (9), 566−78.
(13) Mekahli, D.; Bultynck, G.; Parys, J. B.; De Smedt, H.; Missiaen, L. Endoplasmic-reticulum calcium depletion and disease. *Cold Spring Harb Perspect Biol.* **2011**, *3* (6), a004317.
(14) Votteler, J.; Sundquist, W. I. Virus budding and the ESCRT pathway. *Cell host & microbe* **2013**, *14* (3), 232−41.
(15) Bieniasz, P. D. Late budding domains and host proteins in enveloped virus release. *Virology* **2006**, *344* (1), 55−63.
(16) Llewellyn, G. N.; Hogue, I. B.; Grover, J. R.; Ono, A. Nucleocapsid promotes localization of HIV-1 gag to uropods that participate in virological synapses between T cells. *PLoS pathogens* **2010**, *6* (10), e1001167.
(17) Sewald, X.; Gonzalez, D. G.; Haberman, A. M.; Mothes, W. In vivo imaging of virological synapses. *Nat. Commun.* **2012**, *3*, 1320.
(18) Igakura, T.; Stinchcombe, J. C.; Goon, P. K.; Taylor, G. P.; Weber, J. N.; Griffiths, G. M.; Tanaka, Y.; Osame, M.; Bangham, C. R. Spread of HTLV-I between lymphocytes by virus-induced polarization of the cytoskeleton. *Science* **2003**, *299* (5613), 1713−6.
(19) Hubner, W.; McNerney, G. P.; Chen, P.; Dale, B. M.; Gordon, R. E.; Chuang, F. Y.; Li, X. D.; Asmuth, D. M.; Huser, T.; Chen, B. K. Quantitative 3D video microscopy of HIV transfer across T cell virological synapses. *Science* **2009**, *323* (5922), 1743−7.
(20) Jolly, C.; Kashefi, K.; Hollinshead, M.; Sattentau, Q. J. HIV-1 cell to cell transfer across an Env-induced, actin-dependent synapse. *J. Exp Med.* **2004**, *199* (2), 283−93.
(21) Llewellyn, G. N.; Grover, J. R.; Olety, B.; Ono, A. HIV-1 Gag associates with specific uropod-directed microdomains in a manner dependent on its MA highly basic region. *Journal of virology* **2013**, *87* (11), 6441−54.
(22) Chen, A. K.; Sengupta, P.; Waki, K.; Van Engelenburg, S. B.; Ochiya, T.; Ablan, S. D.; Freed, E. O.; Lippincott-Schwartz, J. MicroRNA binding to the HIV-1 Gag protein inhibits Gag assembly and virus production. *Proc. Natl. Acad. Sci. U.S.A.* **2014**, *111* (26), E2676−83.
(23) Tanwar, H. S.; Khoo, K. K.; Garvey, M.; Waddington, L.; Leis, A.; Hijnen, M.; Velkov, T.; Dumsday, G. J.; McKinstry, W. J.; Mak, J. The thermodynamics of Pr55Gag-RNA interaction regulate the assembly of HIV. *PLoS pathogens* **2017**, *13* (2), e1006221.
(24) Lutomski, C. A.; Lyktey, N. A.; Zhao, Z.; Pierson, E. E.; Zlotnick, A.; Jarrold, M. F. Hepatitis B Virus Capsid Completion Occurs through Error Correction. *J. Am. Chem. Soc.* **2017**, *139* (46), 16932−16938.
(25) Lutomski, C. A.; Lyktey, N. A.; Pierson, E. E.; Zhao, Z.; Zlotnick, A.; Jarrold, M. F. Multiple Pathways in Capsid Assembly. *J. Am. Chem. Soc.* **2018**, *140* (17), 5784−5790.
(26) Cheng, H.; Lederer, W. J.; Cannell, M. B. Calcium sparks: elementary events underlying excitation-contraction coupling in heart muscle. *Science* **1993**, *262* (5134), 740−4.
(27) Klein, M. G.; Cheng, H.; Santana, L. F.; Jiang, Y. H.; Lederer, W. J.; Schneider, M. F. Two mechanisms of quantized calcium release in skeletal muscle. *Nature* **1996**, *379* (6564), 455−458.
(28) Nelson, M. T.; Cheng, H.; Rubart, M.; Santana, L. F.; Bonev, A. D.; Knot, H. J.; Lederer, W. J. Relaxation of arterial smooth muscle by calcium sparks. *Science* **1995**, *270* (5236), 633−7.
(29) Yao, Y.; Choi, J.; Parker, I. Quantal puffs of intracellular Ca2+ evoked by inositol trisphosphate in Xenopus oocytes. *Journal of physiology* **1995**, *482*, 533−553.
(30) De Crescenzo, V.; ZhuGe, R.; Velázquez-Marrero, C.; Lifshitz, L. M.; Custer, E.; Carmichael, J.; Lai, F. A.; Tuft, R. A.; Fogarty, K. E.; Lemos, J. R.; Walsh, J. V. Ca2+ Syntillas, Miniature Ca2+ Release Events in Terminals of Hypothalamic Neurons, Are Increased in Frequency by Depolarization in the Absence of Ca2+ Influx. *J. Neurosci.* **2004**, *24* (5), 1226−1235.
(31) Berridge, M. J.; Lipp, P.; Bootman, M. D. The versatility and universality of calcium signalling. *Nat. Rev. Mol. Cell Biol.* **2000**, *1* (1), 11−21.
(32) Sundquist, W. I.; Krausslich, H. G. HIV-1 assembly, budding, and maturation. *Cold Spring Harbor perspectives in medicine* **2012**, *2* (7), a006924.
(33) Freed, E. O. HIV-1 assembly, release and maturation. *Nat. Rev. Microbiol* **2015**, *13* (8), 484−96.
(34) Campbell, S.; Rein, A. In vitro Assembly Properties of Human Immunodeficiency Virus Type 1 Gag Protein Lacking the p6 Domain. *J. Virol.* **1999**, *73* (3), 2270−2279.
(35) Grabarek, Z. Structural basis for diversity of the EF-hand calcium-binding proteins. *J. Mol. Biol.* **2006**, *359* (3), 509−25.
(36) Kurokawa, H.; Osawa, M.; Kurihara, H.; Katayama, N.; Tokumitsu, H.; Swindells, M. B.; Kainosho, M.; Ikura, M. Target-induced conformational adaptation of calmodulin revealed by the crystal structure of a complex with nematode Ca(2+)/calmodulin-dependent kinase kinase peptide. *J. Mol. Biol.* **2001**, *312* (1), 59−68.
(37) Zhou, Q.; Zhou, P.; Wang, A. L.; Wu, D.; Zhao, M.; Sudhof, T. C.; Brunger, A. T. The primed SNARE-complexin-synaptotagmin complex for neuronal exocytosis. *Nature* **2017**, *548* (7668), 420−425.
(38) Gottwein, E.; Krausslich, H. G. Analysis of human immunodeficiency virus type 1 gag ubiquitination. *Journal of virology* **2005**, *79* (14), 9134−44.
(39) Ott, D. E.; Coren, L. V.; Copeland, T. D.; Kane, B. P.; Johnson, D. G.; Sowder, R. C., II; Yoshinaka, Y.; Oroszlan, S.; Arthur, L. O.; Henderson, L. E. Ubiquitin Is Covalently Attached to the p6gag Proteins of Human Immunodeficiency Virus Type 1 and Simian Immunodeficiency Virus and to the $p12^{Gag}$ Protein of Moloney Murine Leukemia Virus. *J. Virol.* **1998**, *72* (4), 2962−2968.
(40) Lecker, S. H.; Goldberg, A. L.; Mitch, W. E. Protein degradation by the ubiquitin-proteasome pathway in normal and disease states. *J. Am. Soc. Nephrol* **2006**, *17* (7), 1807−19.
(41) Ott, D. E.; Coren, L. V.; Chertova, E. N.; Gagliardi, T. D.; Schubert, U. Ubiquitination of HIV-1 and MuLV Gag. *Virology* **2000**, *278* (1), 111−21.
(42) Schmidt, F.; Weisblum, Y.; Muecksch, F.; Hoffmann, H. H.; Michailidis, E.; Lorenzi, J. C. C.; Mendoza, P.; Rutkowska, M.; Bednarski, E.; Gaebler, C.; Agudelo, M.; Cho, A.; Wang, Z.; Gazumyan, A.; Cipolla, M.; Caskey, M.; Robbiani, D. F.; Nussenzweig, M. C.; Rice, C. M.; Hatziioannou, T.; Bieniasz, P. D. Measuring SARS-CoV-2 neutralizing antibody activity using pseudotyped and chimeric viruses. *J. Exp Med.* **2020**, *217* (11), e20201181.
(43) Friedrich, M.; Setz, C.; Hahn, F.; Matthaei, A.; Fraedrich, K.; Rauch, P.; Henklein, P.; Traxdorf, M.; Fossen, T.; Schubert, U. Glutamic Acid Residues in HIV-1 p6 Regulate Virus Budding and Membrane Association of Gag. *Viruses* **2016**, *8* (4), 117.
(44) Hill, M.; Tachedjian, G.; Mak, J. The packaging and maturation of the HIV-1 Pol proteins. *Curr. HIV Res.* **2005**, *3* (1), 73−85.
(45) Carlson, L. A.; Briggs, J. A.; Glass, B.; Riches, J. D.; Simon, M. N.; Johnson, M. C.; Muller, B.; Grunewald, K.; Krausslich, H. G. Three-dimensional analysis of budding sites and released virus suggests a revised model for HIV-1 morphogenesis. *Cell host & microbe* **2008**, *4* (6), 592−9.
(46) Bohannon, K. P.; Hanson, P. I. ESCRT puts its thumb on the nanoscale: Fixing tiny holes in endolysosomes. *Curr. Opin Cell Biol.* **2020**, *65*, 122−130.
(47) Pang, Z. P.; Sudhof, T. C. Cell biology of Ca2+-triggered exocytosis. *Curr. Opin Cell Biol.* **2010**, *22* (4), 496−505.

https://doi.org/10.1021/jacsau.1c00563
JACS Au 2022, 2, 522−530